Enhancing Thermoelectric Performance of Bi 2 Te 3 -based Nanostructures through Rational Structure Design

Article *in* Nanoscale · March 2016

DOI: 10.1039/C6NR00719H

CITATION
1

READS
76

4 authors:

Min Hong
University of Queensland
16 PUBLICATIONS **79** CITATIONS
SEE PROFILE

Zhi-Gang Chen
University of Southern Queensland
159 PUBLICATIONS **6,783** CITATIONS
SEE PROFILE

Lei Yang
University of Queensland
33 PUBLICATIONS **338** CITATIONS
SEE PROFILE

Jin Zou
University of Queensland
715 PUBLICATIONS **16,172** CITATIONS
SEE PROFILE

Some of the authors of this publication are also working on these related projects:

Developing high-performance thermoelectric materials through nanostructuring and band engineering View project

TiO2 nanotube for gas sensor View project

Nanoscale

Accepted Manuscript

This article can be cited before page numbers have been issued, to do this please use: M. Hong, Z. G. Chen, L. Yang and J. Zou, *Nanoscale*, 2016, DOI: 10.1039/C6NR00719H.

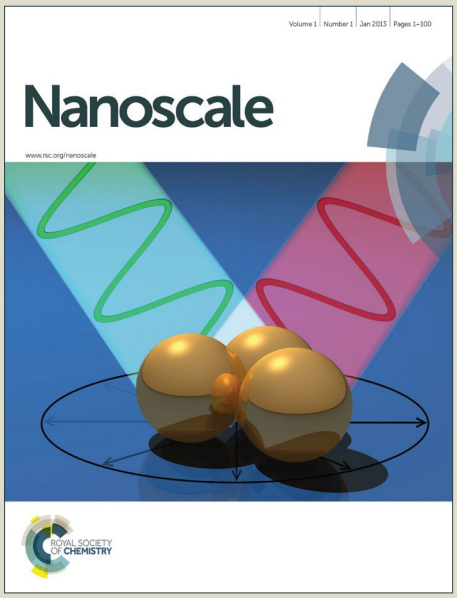

ROYAL SOCIETY OF CHEMISTRY

www.rsc.org/nanoscale

ROYAL SOCIETY OF CHEMISTRY View Article Online
DOI: 10.1039/C6NR00719H

Journal Name

ARTICLE

Enhancing Thermoelectric Performance of Bi_2Te_3-based Nanostructures through Rational Structure Design

Received 00th January 20xx,
Accepted 00th January 20xx

DOI: 10.1039/x0xx00000x

www.rsc.org/

Min Hong[a], Zhi-Gang Chen*[a], Lei Yang[a] and Jin Zou*[ab]

Nanostructuring has been successfully employed to enhance the thermoelectric performance of Bi_2Te_3 due to their obtained low thermal conductivity. In order to further reduce the thermal conductivity, we design a hierarchical nanostructures assembled with well-aligned Bi_2Te_3 nanoplates using Te nanotubes as templates by a facial microwave-assisted solvothermal synthesis. From the comparisons of their thermoelectric performance and theoretical calculations with simple Bi_2Te_3 nanostructures, we found that Te/Bi_2Te_3 hierarchical nanostructures exhibits higher figure-of-merit due to the optimized reduced Fermi level and enhanced phonon scattering, as well as the suppressed bipolar conduction. This study provides an effective approach to enhance thermoelectric performance of Bi_2Te_3 based nanostructures by rationally designing the nanostructures.

Introduction

Considering the environmental pollution caused by the consumption of fossil fuels and the rising demand of energy depletion, it is necessary to develop green sustainable energy sources and energy harvesting technologies.[1] Thermoelectric materials, enabling the direct conversion between heat and electricity, provide an alternative solution to these crises.[2] The energy conversion efficiency of a thermoelectric material is gauged by the dimensionless figure of merit, $ZT = S^2\sigma T/\kappa$, where S, σ, κ and T are the Seebeck coefficient, electrical conductivity, thermal conductivity (including electronic component κ_e, lattice component κ_l, and bipolar component κ_{bi}), and the working temperature, respectively.[3-5] However, the current low ZT values, especially for n-type (with free electrons) thermoelectric materials, significantly hinder the commercialization of thermoelectric devices, which demand the synergistic development of both n-type and p-type (with free holes) thermoelectric elements.[6,7]

Bi_2Te_3 and the family of similar compounds are the promising thermoelectric candidates at room temperature region.[8-10] Because of their six valley degeneracy, the narrow energy gap and layered crystal structure, Bi_2Te_3 potentially meets the criteria of high power factor ($S^2\sigma$) and low κ.[11] Compared with bulk counterpart, nanostructured Bi_2Te_3 can achieve much lower κ, and provides promising possibilities to manipulate the thermoelectric properties.[12] Especially, rhombohedral structured Bi_2Te_3 nanoplates, as two-dimensional nanostructures,[13-15] exhibit strengthened phonon scattering due to the dense grain boundaries after sintered into pellets.[16] To further strengthen the phonon scattering, we can assemble the randomly orientated nanoplates in the form of well-aligned hierarchical nanostructures.[17]

Inspired by our previous study on epitaxial growth of T-shaped Te/Bi_2Te_3 heteronanojunctions,[18] we explored the fabrication of the hierarchical nanostructures by using the one-dimensional Te nanostructures as templates. One-dimensional Te nanostructures, including nanowires[19] and nanotubes[20,21] have been reported to be synthesized by the wet chemical method. Compared with nanowires, nanotubes show even lower κ due to the existence of tube channels.[22] Because of the potential lattice match between trigonal structured Te (a_{Te} = 4.45 Å, c_{Te} = 5.92 Å)[23] and rhombohedral structured Bi_2Te_3 (a_{Bi2Te3} = 4.38 Å, c_{Bi2Te3} = 30.49 Å)[24], i.e. $a_{Te} \approx a_{Bi2Te3}$, $c_{Te} \approx 1/5\ c_{Bi2Te3}$, it is anticipated a small lattice mismatch of $\{11\bar{2}0\}$ plane for Te and Bi_2Te_3 (< 2%),[25] so that $\{11\bar{2}0\}$ planes of Te nanotubes can serve as templates for the epitaxial growth of Bi_2Te_3 nanoplates, as demonstrated in the atomic models of Te/Bi_2Te_3 heteronanojunctions (refer to Fig. 1a and b). Using this crystallographic relationship, Te/Bi_2Te_3 hierarchical nanostructures can be formed on Te nanostructures. For layered Bi_2Te_3 single crystals, κ is anisotropic and its value along the c-axis is only ~50% of that on the a-b plane,[26] so that massive studies have explored the advantage of well-aligned Bi_2Te_3 layered nanostructures to reduce κ.[7,19,27] Therefore, this hierarchical nanostructures is expected to result in significantly

[a] Materials Engineering, University of Queensland, Brisbane, QLD 4072, Australia.
[b] Centre for Microscopy and Microanalysis, University of Queensland, Brisbane, QLD 4072, Australia.
Email: j.zou@uq.edu.au, z.chen1@uq.edu.au.

† Electronic Supplementary Information (ESI) available: XRD pattern, SEM,and TEM images of as-synthesized Te nanotubes, See DOI: 10.1039/x0xx00000x

View Article Online
DOI: 10.1039/C6NR00719H

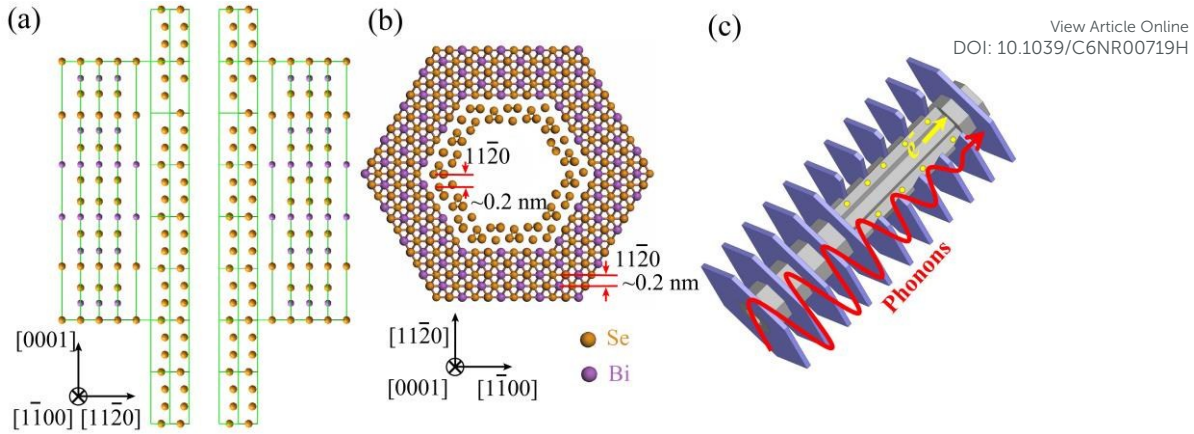

Fig. 1 Schematic atomic models for Te/Bi_2Te_3 hierarchical nanostructures showing the crystallographic relationship along (a) [1$\bar{1}$00] and (b) [0001]. (c) Schematic demonstrating the advantages of the hierarchical nanostructure in strengthening phonon scattering and ensuring high electrical conductivity.

enhanced phonon scattering, as schematically illustrated in Fig. 1c. On the other hand, the crystalline nature of Te nanotube walls may enhance σ.[22,28]

In this study, we employed a microwave-assisted solvothermal method to synthesize Te/Bi_2Te_3 hierarchical nanostructures using Te nanotubes as templates. To confirm the superiority of Te/Bi_2Te_3 hierarchical nanostructures in enhancing thermoelectric efficiency, highly uniform Bi_2Te_3 nanoplates were also investigated as a reference. Through the comparison of the morphology-dependent thermoelectric performance, we fundamentally studied the structural effects on tuning thermoelectric properties.

Experimental

Materials Synthesis and Processing

In this study, analytical grade $Bi(NO_3)_3{\cdot}5H_2O$, Na_2TeO_3, ethylene glycol, poly(N-vinyl-2-pyrrolidone) (PVP, M_w = 4000), and NaOH solution were used as precursors.

The synthesis of the Te/Bi_2Te_3 hierarchical nanostructures was carried out in two steps. The first step is to synthesize Te nanotubes as the precursors, following by the second step - synthesis of Te/Bi_2Te_3 hierarchical nanostructures. In the first step, we added 332.4 mg Na_2TeO_3 and 0.2 g PVP into 40 mL ethylene glycol. The solutions were stirred vigorously for 30 min at room temperature. Subsequently, the obtained clear solutions were sealed in a 100 mL teflon vessel, which was heated in a CEM Mars-6 microwave oven at 230 ˚C for 5 min. After naturally cooled to room temperature, the as-synthesized Te nanotubes were collected by a high-speed centrifugation, washed six times with distilled water and absolute ethanol and finally dried at 60 ˚C for 12 h in a vacuum oven. In the second step, the obtained Te nanotubes were mixed with $Bi(NO_3)_3{\cdot}5H_2O$ into 40 mL ethylene glycol with a mole ratio of 2:3, and with NaOH solution (5 mol/L, 2 mL). After stirring for ~30 min, the mixed solution was transferred into the teflon vessels again, and heated in the CEM Mars-6 microwave oven at 230 ˚C for 5 min. In the second step, NaOH with low concentration enables the gentle dissolution of Te from their external size walls to allow the epitaxial growth of Bi_2Te_3 nanoplates through the entire body of the Te nanotubes.[29] Through washing, centrifuging and drying, we obtained the final nanopowders.

As a comparison, pure Bi_2Te_3 nanoplates were also synthesized. During the synthesis, 485.1 mg $Bi(NO_3)_3{\cdot}5H_2O$, 332.4 mg Na_2TeO_3 and 0.2 g PVP were mixed with 40 mL ethylene glycol and NaOH solution (5 mol/L, 2mL). After being stirred vigorously, the obtained clear solutions were sealed in the teflon vessel, and heated in the CEM Mars-6 microwave oven at 230 ˚C for 5 min. After naturally cooled to room temperature, the synthesized products were collected by a high-speed centrifugation, washed six times with distilled water and absolute ethanol, and finally dried at 60 ˚C for at least 12 h in a vacuum oven.

Materials Characterizations

The phase purities of the as-synthesized products were examined by the X-ray diffractometer (XRD) equipped with graphite monochromatized, Cu $K\alpha$ radiation (λ = 1.5418 Å). The morphological, structural, and compositional characteristics of the synthesized products were investigated by scanning electron microscopy (SEM, JEOL 7800) and transition electron microscopy (TEM, FEI F20), equipped with EDS for compositional analysis.

Fabrication of Pellets

The as-synthesized Te/Bi_2Te_3 hierarchical nanostructures and Bi_2Te_3 nanoplates were compressed by the spark plasma sintering (SPS) under 40 MPa and at 250 ˚C for 5 min in vacuum into pellets with a diameter of 12.5 mm and a thickness of 2 mm. The densities (d) of sintered pellets were measured by an Archimedes method, and confirmed to be over 90%.

Thermoelectric Performance Measurement

Thermal diffusivity (D) of sintered pellets was measured by a laser flash method (LFA 457, NETZSCH), and κ was calculated through $\kappa=DC_pd$, where C_p is the specific heat capacity. C_p is obtained from empirical formulas C_{pBT} = 108.06+5.53×10^{-2}T JK^{-1}mol^{-1} for Bi_2Te_3.[30] σ and S were measured simultaneously on a ZEM-3, ULVAC. The uncertainties of the thermoelectric performance measurements (S, σ and D) were estimated as ~5% for each.

Results and discussion

Fig. 2a is the X-ray diffraction (XRD) pattern collected from the as-synthesized Te/Bi_2Te_3 nanopowders with the inset showing its enlarged view of 2θ in the range of 34° – 43°. As can be seen, the diffraction peaks can be indexed as the rhombohedral structured Bi_2Te_3 phase with lattice parameters of a = 4.38 Å and c = 30.49 Å (JCPDS No. 89-2009)[24] and the trigonal structured Te phase with lattice parameters of a = 4.45 Å and c = 5.92 Å (JCPDS No. 36-1452).[23] It should be noted that no Bi contamination was detected in the as-prepared samples, although our samples contain excessive Bi^{3+} (dissolved from $Bi(NO_3)_35H_2O$). We believe that the excessive Bi^{3+} was still in the solvent after the synthesis that was washed away during the post-synthesis process. Fig. 2b is a SEM image, and shows that the majority (> 90%) of synthesized products are rod-like nanostructures. Fig. 2c is a TEM image of a typical rod-like nanostructure, in which the feature of a hierarchical nanostructure is seen — many parallel nanoplates are linked by a nanotube (as a stem). Their crystallographic relationship was further analyzed using selected area electron diffraction (SAED) and high resolution TEM (HRTEM). Fig. 2d is a SAED pattern taken from the circled area of such hierarchical nanostructure showing superimposed [1 $\bar{1}$ 00] zone-axis diffraction patterns of a trigonal structured Te phase and a rhombohedral structured Bi_2Te_3 phase, from which the crystallographic relationship between the Te nanotube and the Bi_2Te_3 nanoplates can be determined as $[0001]_{Te}$ // $[0001]_{Bi2Te3}$ and $[\,11\bar{2}\,0]_{Te}$ // $[\,11\bar{2}\,0]_{Bi2Te3}$. Fig. 2e and f are the corresponding HRTEM images taken from the arrowed nanotube body and the nanoplate edge, respectively, which further suggests the coexistence of a high-crystalline trigonal structured Te nanotube stem and rhombohedral structured Bi_2Te_3 nanoplate. EDS was applied to examine the compositions of the nanotube and nanoplates. Fig. 2g shows the EDS profiles collected respectively from the labeled areas in Fig. 2c, suggesting that the nanotube is indeed Te, while the nanoplates are composed of Bi and Te with a mole ratio of approximately 2:3. To understand the structural characteristics of Te/Bi_2Te_3 hierarchical nanostructures, we examined structures of Te nanotubes after first step synthesis (an example is shown in the ESI), which demonstrated that the

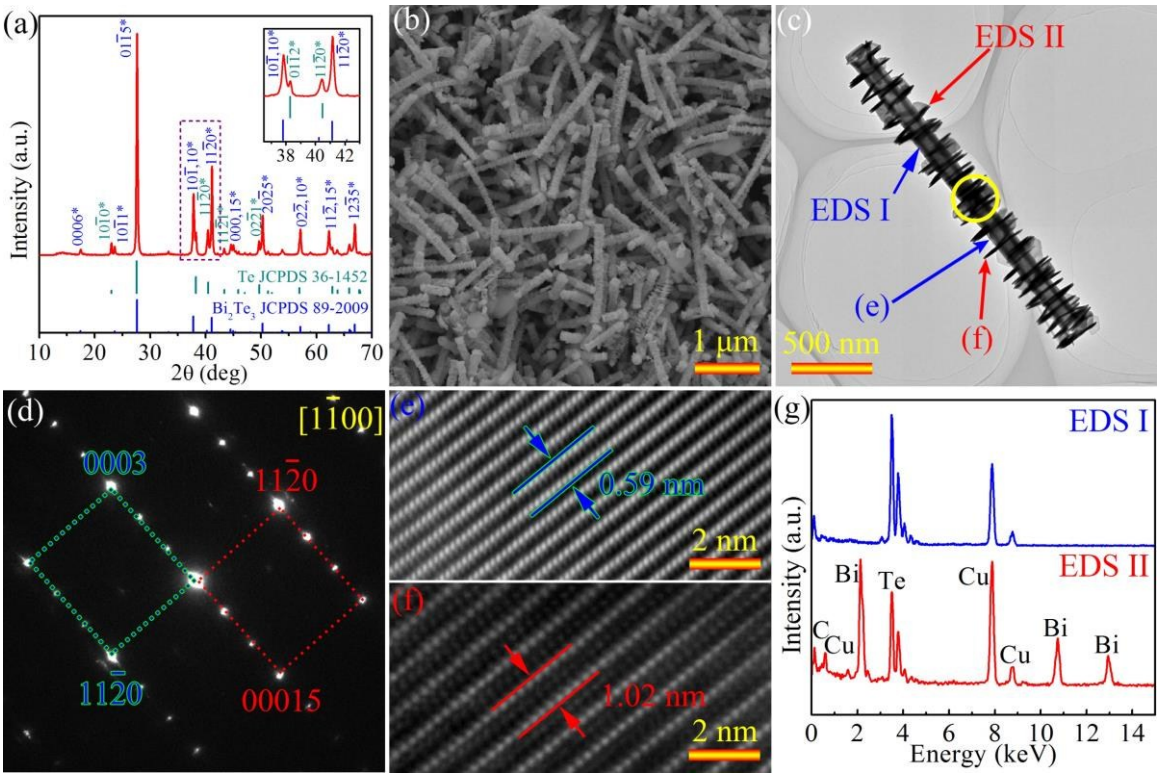

Fig. 2 (a) XRD patterns collected from as-synthesized Te/Bi2Te3 nanopowders with inset showing its enlarged view. (b) Low-magnification SEM image showing a large amount of hierarchical nanostructures. (c) TEM image of a typical Te/Bi2Te3 hierarchical nanostructure. (d) The [1$\bar{1}$00] zone-axis SAED. (e) and (f) HRTEM images respectively taken from the arrowed areas in (c). (g) EDS profiles respectively taken from the arrowed areas in (c).

obtained nanotubes have their lengths of 2 - 6 μm and diameters of 100 - 200 nm. Our extensive electronic microscopy investigations of Te/Bi_2Te_3 hierarchical nanostructures indicate that the lateral size and thickness of the epitaxially grown Bi_2Te_3 nanoplates are relatively independent to the diameters of Te nanotubes.

As a comparison, Bi_2Te_3 nanoplates were also synthesized and characterized. Fig. 3a is a XRD pattern of as-prepared Bi_2Te_3 nanoplates, confirming Bi_2Te_3 nanoplates are highly pure rhombohedral structured Bi_2Te_3 phase. Fig. 3b is the low-magnification SEM image of as-synthesized Bi_2Te_3 hexagonal-shaped nanoplates that have uniform morphology with their lateral size of ~1μm. The inset of Fig. 3b is the high-magnification SEM image showing the side-view of several nanoplates, from which the nanoplate thickness of ~20 nm can be revealed. Fig. 3c is the TEM image of a typical nanoplate with lateral size of ~1μm, in accordance with the size determined by SEM (refer to Fig. 3b). Fig. 3d is the [0001] zone-axis SAED pattern and Fig. 3e is the corresponding HRTEM image with a lattice spacing of 0.22 nm, which matches well with the d value of the $\{11\bar{2}0\}$ planes of rhombohedral structured Bi_2Te_3.[31] Fig. 3f shows the EDS profile, indicating that the elemental ratio of Bi and Te is approximately 2:3 (note that Cu and C peaks are caused by the TEM Cu grid with C supporting films).

In order to evaluate their thermoelectric performance, we examined sintered pellets made from Te/Bi_2Te_3 hierarchical nanostructures and Bi_2Te_3 nanoplates. Fig. 4a presents σ and S as a function of temperature, indicated by the left-hand side and the right-hand side y-axis, respectively. As can be seen, σ declines from ~8×10^4 Sm^{-1} to ~5×10^4 Sm^{-1} with increasing the temperature for both Bi_2Te_3 and Te/Bi_2Te_3 based pellets; however the declining trend in Te/Bi_2Te_3 is mitigated. In the case of S, its negative sign for both Bi_2Te_3 and Te/Bi_2Te_3 cases indicates their n-type feature. Specifically, S for Bi_2Te_3 ranges from -150 μVK^{-1} to -170 μVK^{-1}, while that for Te/Bi_2Te_3 fluctuates between -165 μVK^{-1} and -182 μVK^{-1} in the studied temperature range. Moreover, the absolute value of S increases first and then decreases with increasing the temperature. The decrease in $|S|$ should be caused by the bipolar conduction,[32] and the peak of $|S|$ for Te/Bi_2Te_3 shifts towards the higher temperature, suggesting that the bipolar conduction is suppressed at the higher temperature. Based on the measured σ and S, we can calculate $S^2\sigma$, and plotted in Fig. 4b as a function of temperature. As can be seen, the peak $S^2\sigma$ of 19.2×10^{-4} $Wm^{-1}K^{-2}$ for Te/Bi_2Te_3 is larger than that of 18×10^{-4} $Wm^{-1}K^{-2}$ for Bi_2Te_3, and the peak $S^2\sigma$ for Te/Bi_2Te_3 shifts to higher temperature. This is due to the suppressed bipolar conduction and the mitigated declining trend in σ with increasing the temperature in Te/Bi_2Te_3 (refer to Fig. 4a).

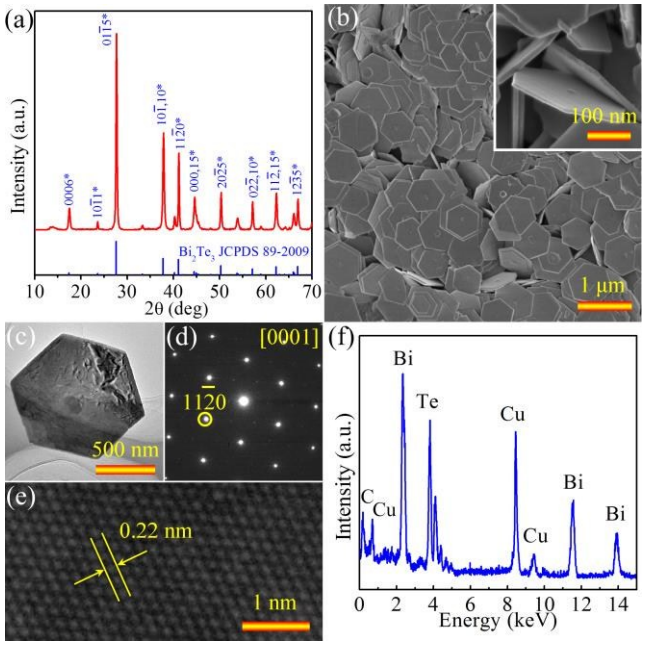

Fig. 3 (a) XRD pattern taken from the as-synthesized Bi_2Te_3 nanopowders (b) Low-magnification SEM image with inset of side-view high-magnification SEM image. (c) TEM image of a typical Bi_2Te_3 nanoplate. (d), (e), and (f) Corresponding SAED pattern, HRTEM image, and EDS profile, respectively.

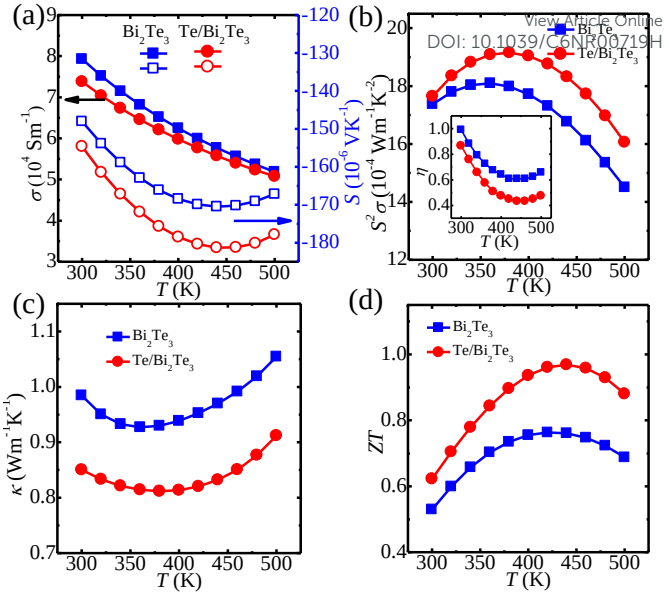

Fig. 4 Thermoelectric properties of Te/Bi_2Te_3 hierarchical nanostructures compared with Bi_2Te_3 nanoplates (a) σ and S, (b) $S^2\sigma$ with inset showing calculated η, (c) κ and (d) ZT.

To understand the enhanced $S^2\sigma$, we calculated the reduced Fermi level ($\eta=E_f/k_BT$, with E_f representing the Fermi level and k_B is the Boltzmann constant) based on the measured S by using the following equation[33]

$$S = -\frac{k_B}{e}\left[\frac{2F_1(\eta)}{F_0(\eta)} - \eta\right], \quad (1)$$

with the generalized Fermi integral

$$F_i(\eta) = \int_0^\infty \frac{\varepsilon^i}{1+\exp(\varepsilon-\eta)} d\varepsilon \ ; \quad (2)$$

where e is the elementary charge. The inset of Fig. 4b plots the variation of η with temperature for both Bi_2Te_3 and Te/Bi_2Te_3

in which η for Te/Bi_2Te_3 is smaller than that for Bi_2Te_3. According to our previous study,[34] to maximize $S^2\sigma$, the Fermi level should locate near the conduction band edge for n-type thermoelectric materials. Compared with Bi_2Te_3, η for Te/Bi_2Te_3 is closer to its conduction band edge, so that an enhanced $S^2\sigma$ for Te/Bi_2Te_3 can be anticipated. The η decline for Te/Bi_2Te_3 nanostructures can be ascribed to the excessive Te (provided by Te nanotube stems), which might suppress the Te vacancies in epitaxially grown Bi_2Te_3 nanoplates. Te vacancies in Bi_2Te_3 are generally unavoidable (giving n-type transport feature), and the Te vacancies lead to the Fermi level residing deep in the conduction band. Favourably, by adding more Te, Te vacancies in in Bi_2Te_3 can be supressed; resulting in the shift of the Fermi level towards the valance band in our Te/Bi_2Te_3 nanostructures. Fig. 4c plots κ versus temperature, from which κ in Te/Bi_2Te_3 shows ~20% reduction than that for Bi_2Te_3. Due to the enlarged $S^2\sigma$ and simultaneously decreased κ, ZT for Te/Bi_2Te_3 is enhanced, as shown in Fig. 4d. ZT for Te/Bi_2Te_3 reaches ~1, much larger than that of ~ 0.75 for Bi_2Te_3.

From above discussion, one of the critical reasons for enhanced ZT is the significantly decreased κ. To clarify the underlying principle, we studied the contributions of κ from electrons, phonons and bipolar conduction. According to the Wiedemann-Franz law,[35] κ_e can be expressed as

$$\kappa_e = L\sigma T, \quad (3)$$

where L is the Lorenz number. Employing the single Kane band model, L can be determined by[36]

$$L = \left(\frac{k_B}{e}\right)^2 \left[\frac{3F_2(\eta)}{F_0(\eta)} - \left(\frac{2F_1(\eta)}{F_0(\eta)}\right)^2\right] \quad (4)$$

Through inputting the determined η (refer to the inset of Fig. 4b) into Equation (4), we can calculate L. The results are shown in Fig. 5a, in which L fluctuates around 1.6×10^{-8} V^2K^{-2} for both samples, matching with reported values for nanostructured thermoelectric systems.[37] On this basis, Fig. 5b plots the calculated κ_e over the studied temperature, where κ_e is reduced in Te/Bi_2Te_3 due to its smaller σ and L over Bi_2Te_3. By subtracting κ_e from κ, we can study the variation of κ_l, although there is a κ_{bi} contribution at high temperature. Fig. 4b shows the obtained temperature dependent κ-κ_e, which suggests that κ_l in Te/Bi_2Te_3 is significantly decreased. This is because Te/Bi_2Te_3 hierarchical nanostructures have the well-aligned nanoplates attached on the body surface, which lead to stronger phonon scattering compared with the randomly orientated Bi_2Te_3 nanoplates.[38] Moreover, κ_{bi} is calculated using the reference-outlined method.[39] Specifically, by extrapolating the linear relationship between κ_l and $1/T$ demonstrated in the insert of Fig. 5c, we can obtain κ_l in the entire studied temperature range, and finally, though subtracting κ_l from κ-κ_e, we can obtain κ_{bi}. Fig. 5d shows the determined κ_{bi} as a function of temperature. As can be seen, κ_{bi} for Te/Bi_2Te_3 is reduced; suggesting that the bipolar conduction in Te/Bi_2Te_3 has been indeed suppressed, which is consistent with the peak of S for Te/Bi_2Te_3 shifting to the high temperature (refer to Fig. 4a). To understand this, we note that the band gap difference between Te (0.33 eV)[40] and Bi_2Te_3 (0.15 eV) [41] may lead to an extra energy offset between the conduction and valance bands for the Te/Bi_2Te_3 nanostructures. In addition, our Bi_2Te_3 nanoplates in Te/Bi_2Te_3 are generally thinner than the normal Bi_2Te_3 nanoplates, leading to the enlargement of band gap in our thinner Bi_2Te_3 nanoplates.[42] As a consequence, the bipolar conduction can be suppressed in our Te/ Bi_2Te_3 nanostructures.

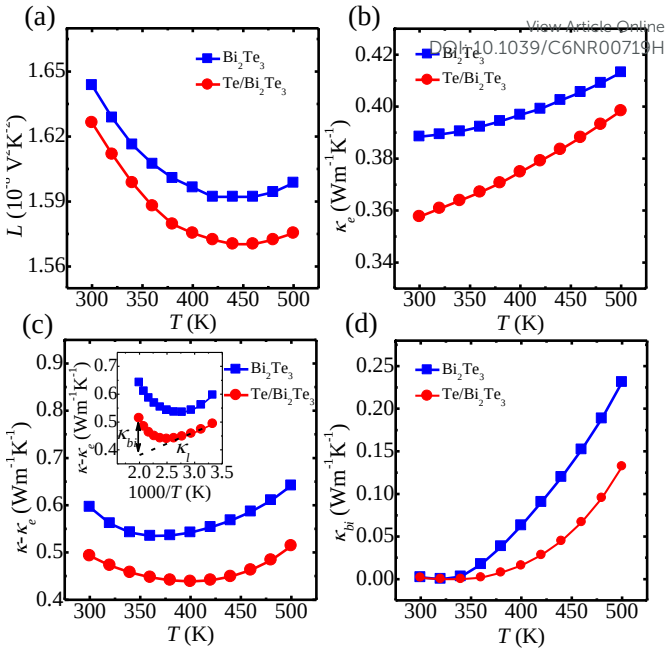

Fig. 5 (a) Calculated temperature dependent (a) L, (b) κ_e, (c) κ - κ_e with inset showing the inverse temperature dependence of κ - κ_e, and (d) κ_{bi}.

Conclusion

We successfully fabricated Te/Bi_2Te_3 hierarchical nanostructures using Te nanotubes as templates by the facial microwave-assisted solvothermal method. Through systematic morphological, structural and compositional characterizations, structural quality and the epitaxial growth of well-aligned Bi_2Te_3 nanoplates on Te nanotube stems are verified. The thermoelectric properties measured from their sintered pellets indicate an increased $ZT \approx 1$ when compared with their pure Bi_2Te_3 nanoplates with $ZT \approx 0.75$. Our modelling studies suggest that the enhanced ZT of our Te/Bi_2Te_3 hierarchical nanostructures is caused by the optimized reduced Fermi level, the strengthened phonon scatterings, and the suppressed bipolar conduction. This study provides an effective approach to enhance thermoelectric efficiency by designing rational nanostructures.

Acknowledgements

This work was financially supported by the Australian Research Council. MH thanks the China Scholarship Council for providing a PhD stipend. The Australian Microscopy & Microanalysis

Research Facility is acknowledged for providing characterization facilities.

Notes and references

1. T. M. Tritt and M. A. Subramanian, *Mrs. Bull.*, 2006, **31**, 188-194.
2. G. J. Snyder and E. S. Toberer, *Nat. Mater.*, 2008, **7**, 105-114.
3. Z.-G. Chen, G. Han, L. Yang, L. Cheng and J. Zou, *Prog. Nat. Sci.*, 2012, **22**, 535-549.
4. L. Yang, Z.-G. Chen, G. Han, M. Hong, Y. Zou and J. Zou, *Nano Energy*, 2015, **16**, 367-374.
5. G. Han, Z.-G. Chen, L. Yang, M. Hong, J. Drennan and J. Zou, *ACS Appl. Mater. Interf.*, 2014, **7**, 989-995.
6. F. J. DiSalvo, *Science*, 1999, **285**, 703-706.
7. H.-C. Chang, C.-H. Chen and Y.-K. Kuo, *Nanoscale*, 2013, **5**, 7017-7025.
8. B. Poudel, Q. Hao, Y. Ma, Y. Lan, A. Minnich, B. Yu, X. Yan, D. Wang, A. Muto, D. Vashaee, X. Chen, J. Liu, M. S. Dresselhaus, G. Chen and Z. Ren, *Science*, 2008, **320**, 634-638.
9. R. J. Mehta, Y. Zhang, C. Karthik, B. Singh, R. W. Siegel, T. Borca-Tasciuc and G. Ramanath, *Nat. Mater.*, 2012, **11**, 233-240.
10. M. Hong, Z. G. Chen, L. Yang and J. Zou, *Nano Energy*, 2016, **20**, 144-155.
11. D. M. Rowe, *CRC handbook of thermoelectrics*, CRC Press, New York, 1995.
12. S. W. Finefrock, H. Yang, H. Fang and Y. Wu, *Annu. Rev. Chem. Biomol. Eng.*, 2015, **6**, null.
13. Y. Zhang, L. P. Hu, T. J. Zhu, J. Xie and X. B. Zhao, *Cryst. Growth Des.*, 2013, **13**, 645-651.
14. H.-W. Tsai, T.-H. Wang, T.-C. Chan, P.-J. Chen, C.-C. Chung, A. Yaghoubi, C.-N. Liao, E. W.-G. Diau and Y.-L. Chueh, *Nanoscale*, 2014, **6**, 7780-7785.
15. L. Guo, H. Yan, Q. Moore, M. Buettner, J. Song, L. Li, P. T. Araujo and H.-T. Wang, *Nanoscale*, 2015, **7**, 11915-11921.
16. A. Soni, Y. Shen, M. Yin, Y. Zhao, L. Yu, X. Hu, Z. Dong, K. A. Khor, M. S. Dresselhaus and Q. Xiong, *Nano Lett.*, 2012, **12**, 4305-4310.
17. W. G. Lu, Y. Ding, Y. X. Chen, Z. L. Wang and J. Y. Fang, *J. Am. Chem. Soc.*, 2005, **127**, 10112-10116.
18. L. Cheng, Z.-G. Chen, L. Yang, G. Han, H.-Y. Xu, G. J. Snyder, G.-Q. Lu and J. Zou, *J. Phys. Chem. C*, 2013, **117**, 12458-12464.
19. H. Fang and Y. Wu, *J. Mater. Chem. A*, 2014, **2**, 6004-6014.
20. B. Mayers and Y. Xia, *Adv. Mater.*, 2002, **14**, 279-282.
21. B. Kim and B.-K. Park, *Electronic Materials Letters*, 2012, **8**, 33-36.
22. D. M. Rowe, *Thermoelectrics Handbook : Macro to Nano*, CRC Press, Hoboken, 2005.
23. J.-M. Song, Y.-Z. Lin, Y.-J. Zhan, Y.-C. Tian, G. Liu and S.-H. Yu, *Cryst. Growth Des.*, 2008, **8**, 1902-1908.
24. S. Nakajima, *J. Phys. Chem. Solids*, 1963, **24**, 479-485.
25. J. L. Mi, N. Lock, T. Sun, M. Christensen, M. Sondergaard, P. Hald, H. H. Hng, J. Ma and B. B. Iversen, *ACS Nano*, 2010, **4**, 2523-2530.
26. M. Carle, P. Pierrat, C. Lahalle-Gravier, S. Scherrer and H. Scherrer, *J. Phys. Chem. Solids*, 1995, **56**, 201-209.
27. W. Shi, S. Yu, P. Liu and W. Fan, *CrystEngComm*, 2013, **15**, 2978-2985.
28. W. Liu, X. Yan, G. Chen and Z. Ren, *Nano Energy*, 2012, **1**, 42-56.
29. Y. Liang, W. Wang, B. Zeng, G. Zhang, Q. He and J. Fu, *Mater. Chem. Phys.*, 2011, **129**, 90-98.
30. K. C. Mills, *Thermodynamic Data for Inorganic Sulphides, Selenides and Tellurides*, Butterworths, London, 1974.
31. L. Cheng, Z.-G. Chen, S. Ma, Z.-D. Zhang, Y. Wang, H.-Y. Xu, L. Yang, G. Han, K. Jack, G. Lu and J. Zou, *J. Am. Chem. Soc.*, 2012, **134**, 18920-18923.
32. S. Wang, G. Tan, W. Xie, G. Zheng, H. Li, J. Yang and X. Tang, *J. Mater. Chem.*, 2012, **22**, 20943-20951.
33. C. L. Chen, H. Wang, Y. Y. Chen, T. Day and G. J. Snyder, *J. Mater. Chem. A*, 2014, **2**, 11171-11176.
34. M. Hong, Z.-G. Chen, L. Yang, G. Han and J. Zou, *Adv. Electron. Mater.*, 2015, **1**, 1500025.
35. J. R. Sootsman, D. Y. Chung and M. G. Kanatzidis, *Angew. Chem. Int. Edit.*, 2009, **48**, 8616-8639.
36. T. Zhu, H. Gao, Y. Chen and X. Zhao, *J. Mater. Chem. A*, 2014, **2**, 3251-3256.
37. L. Zhao, S. H. Lo, J. He, H. Li, K. Biswas, J. Androulakis, C.-I. Wu, T. P. Hogan, D.-Y. Chung, V. P. Dravid and M. G. Kanatzidis, *J. Am. Chem. Soc.*, 2011, **133**, 20476-20487.
38. X. B. Zhao, X. H. Ji, Y. H. Zhang, T. J. Zhu, J. P. Tu and X. B. Zhang, *Appl. Phys. Lett.*, 2005, **86**.
39. W.-S. Liu, B.-P. Zhang, J.-F. Li, H.-L. Zhang and L.-D. Zhao, *J. Appl. Phys.*, 2007, **102**, 103717.
40. V. B. Anzin, M. I. Eremets, Y. V. Kosichkin, A. I. Nadezhdinskii and A. M. Shirokov, *Phys. Status Solidi A*, 1977, **42**, 385-390.
41. D. L. Greenaway and G. Harbeke, *J. Phys. Chem. Solids*, 1965, **26**, 1585-1604.
42. O. V. Yazyev, J. E. Moore and S. G. Louie, *Phys. Rev. Lett.*, 2010, **105**, 266806.

View Article Online
DOI: 10.1039/C6NR00719H

Journal Name

ARTICLE

TOC

Enhancing Thermoelectric Performance of Bi_2Te_3-based Nanostructures through Rational Structure Design

Min Hong[a], Zhi-Gang Chen[*a], Lei Yang[a] and Jin Zou[*ab]

Enhanced thermoelectric performance in Te/Bi_2Te_3 hierarchical nanostructures caused by strengthened phonon scattering, optimized Fermi level, and suppressed bipolar conduction